Materials Research Express

PAPER • **OPEN ACCESS**

Antibacterial Ti-Cu alloy with enhanced mechanical properties as implant applications

To cite this article: ChangBo Yi *et al* 2020 *Mater. Res. Express* **7** 105404

Materials Research Express

PAPER

Antibacterial Ti-Cu alloy with enhanced mechanical properties as implant applications

ChangBo Yi[1], **ZunYun Ke**[1], **Lei Zhang**[2], **Jun Tan**[3,4], **YeHua Jiang**[1] **and ZhengYuan He**[1,*]

[1] School of Materials Science and Engineering, Kunming University of Science and Technology, Kunming, 650093, People's Republic of China
[2] Department of Mechanical & Industrial Engineering, Northeastern University, Boston, MA02115, United States of America
[3] College of Materials science and Engineering, Chongqing University, Chongqing, 400044, People's Republic of China
[4] IFW Dresden, Institute for Complex Materials, PO Box 27 01 16, D-01171 Dresden, Germany
[*] Author to whom any correspondence should be addressed.

E-mail: hzy-810@163.com

Keywords: Ti-Cu alloy, microstructure, mechanical properties, corrosion resistance, antibacterial property.

OPEN ACCESS

RECEIVED
7 September 2020

REVISED
9 October 2020

ACCEPTED FOR PUBLICATION
21 October 2020

PUBLISHED
30 October 2020

Abstract

The service life as hard tissue implantation for clinical application needs compatible mechanical properties, *e.g.* strength, modulus, etc, and certain self-healing in case of internal infection. Therefore, for sake of improving the properties of Ti-Cu alloy, the microstructure, mechanical properties, corrosion resistance and antibacterial properties of Ti-*x*Cu alloy ($x = 2, 5, 7$ and 10 wt.%) prepared by Ar-arc melting followed by heat treatment were studied. The results show that the Ti-Cu alloy was mainly composed of α-Ti matrix and precipitated Ti_2Cu phase. The Cu element mainly accumulates in the lamellar structure and forms the precipitated Ti_2Cu phase. As the increase of Cu content, the lamellar Ti_2Cu phase increases, the compressive strength and elastic modulus also were altered. The Ti-7Cu alloy exhibited the higher compressive strength (2169 MPa) and the lower elastic modulus (108 GPa) compared with other Ti-Cu alloys. The corrosion resistance of Ti-*x*Cu alloys increases with the increase of Cu content. When the Cu content was greater than 5 wt.%, the value of corrosion current density for Ti-Cu alloy was less than 1 $\mu A \cdot cm^{-2}$, which is also significantly lower than that of CP-Ti. The antibacterial test revealed that only the Ti-Cu alloy with 5 wt.% or greater Cu content could display a strong antibacterial rate against *E. coli* and *S. aureus*. Therefore, the prepared Ti-7Cu alloy via heat treatment showed excellent mechanical properties, corrosion resistance, and antibacterial properties, which would meet the replacement of human hard tissue and clinical applications.

1. Introduction

With the rapid development of modern biotechnology, Titanium (Ti) and its alloys had been widespread application in orthopedics and oral cavity repair field for their excellent biocompatibilities, corrosion resistances, and mechanical properties [1]. Currently, Ti and its alloys were considered to have the highest success rate in surgical implant surgery [2]. However, the experiences of clinical applications still presented some challenges. As a kind of inert biomaterial material, Ti and its alloys had no antibacterial activity, some bacteria could also be recognized around implant [3, 4]. The bacterial infection might cause the implant to loosen and eventually cause the implant to fail. Therefore, the postoperative infection was a very tricky clinical problem caused by the bacterial colonies. Fourteen million people worldwide were suffering from postoperative infections every day, and 60% of which were related to the use of medical equipment [5].

Copper (Cu) element, as one of the essential trace elements in human body, had been widely applied due to excellent biocompatibility and antibacterial properties [6–8]. Surface modification methods, such as ion implantation [9], Sol-gel method [10], Vapor deposition [11] and dual magnetron sputtering [12], etc, were used to improve the antibacterial activity of implants. However, due to the exfoliation and dissolution of the coatings,

the release of exfoliated debris into surrounding tissues might cause chronic inflammation, resulting in implant loosening even implantation failure. The Ti-Cu alloy by addition of Cu as alloying element was considered as a candidate implant material with good antibacterial activity [13–15]. However, the mechanical properties of Ti-Cu alloy were also deteriorated significantly, such as strength, fracture strain, modulus, etc [16–18]. Therefore, it was necessary to further improve mechanical properties of Ti-Cu alloy while did not reduce the corrosion and antibacterial properties.

Based on above analysis, the Cu content and preparation process for Ti-Cu not only affected the mechanical properties of the alloy, but also determined the antibacterial activity. The study on Ti-Cu alloy with good comprehensive properties was always desired. Therefore, the microstructure, mechanical properties, corrosion resistance and antibacterial properties of Ti-Cu alloy were prepared by combining Ar-arc melting with heat treatment were studied.

2. Experimental

2.1. Preparation of Ti-Cu alloy

High purity Ti ingots (99.995%) and Cu ingots (99.995%) were melted by an Ar-arc melting furnace (DHL-300, China) to prepare Ti-xCu ($x = 2, 5, 7, 10$ wt.%) alloy, respectively. During the melting process, the vacuum in the furnace was pumped to 10^{-3} Pa, and high purity argon (99.999%) was filled into the furnace. Considering the homogeneity of the composition, the ingot was reversed four times per melting. The prepared ingots were treated at 950 °C for 3 h in vacuum furnace, and followed cooling inside the furnace to room temperature. Before testing, all samples were ground on SiC sandpaper with a roughness of up to 2000 grits and polished with a polishing paste of 2.5 μm.

2.2. Phase identification and microstructure

The samples were processed into the dimension of 10 × 10 × 5 mm for phase identification and microstructure analysis. The phase was analyzed by x-ray Diffraction (XRD) (D8 Advance, Bruker, Germany). The morphology was observed by optical microscope and Field Emission Scanning Electron Microscope (SEM, Nova NaNOSEM-450, USA). Electron probe microanalysis (EPMA, JEOL JXA-8230, JEOL Ltd, Tokyo, Japan) was applied to observe the element distribution of the alloy.

2.3. Mechanical performance test

Hardness was measured by HV-1000 Vickers hardness tester (Ningbo, China) with a 300 g load and 10 s dwell time. Five different areas were selected for hardness measurement randomly, and the result was the average with standard deviation. The samples with dimension of Φ4 × 10 mm were machined for compressive tests to measure the strength by a universal testing machine (AG-X 100 KN, Shimadzu Manufacturing Institute, Japan). The elastic modulus of the material was evaluated by the ultrasonic material characterization system (TECLAB, UMS-100, France).

2.4. Electrochemical test

The electrochemical test was completed at CHI660D electrochemical workstation using standard three-electrode system. Ti-Cu alloy samples with size of 10 × 10 × 5 mm were used as the working electrodes. The saturated calomel electrode (SCE) and platinum electrode were used as reference electrode and auxiliary electrode, respectively. Open-circuit potential and dynamic potential polarization curve (Tafel curve) were tested in Hank's solution, containing NaCl 8.00 g, $CaCl_2$ 0.14 g, KCl 0.40 g, $NaHCO_3$ 0.35 g, $MgCl_2{\cdot}H_2O$ 0.01 g, $Na_2HPO_4{\cdot}12H_2O$ 0.06 g, KH_2PO_4 0.06 g, $MgSO_4{\cdot}7H_2O$ 0.06 g and glucose 1.00 g at 37 ± 1 °C, the PH of the solution being about 7 [19]. The open circuit potential (OCP) tests were executed for 1 h to determine the value open-circuit potential (E_{ocp} versus SCE) after immersion for 1 h according to *ISO* 10271:2020 standard. The dynamic potential polarization curve was recorded at a potential range of −1500 ~ 1000 mV, and the potential scanning speed was 1 mV s^{-1}.

2.5. Antibacterial properties

The sample size was Φ4 × 2 mm, which was used for testing the antibacterial properties. The alloy had been verified by the plate count method for *Staphylococcus aureus* (*S. aureus*) and *Escherichia coli* (*E. coli*) antibacterial activity. The test samples (Ti-xCu alloy) and the control sample (CP-Ti) were cultured in 2 ml bacterial suspension diluted 10 times to 105 CFU ml^{-1} concentrations with PBS solution at 37 °C for 24 h under humidity of 90%, respectively. Subsequently, the sample surface was rinsed with 2 ml PBS solution to ensure that there was no bacterial residue on the surface. The washing solution about 0.1 ml was inoculated on nutrient agar plate at 37 °C for 4 h. The viable bacteria were counted by automatic colony counter according to *GB/T* 4789.2–2010

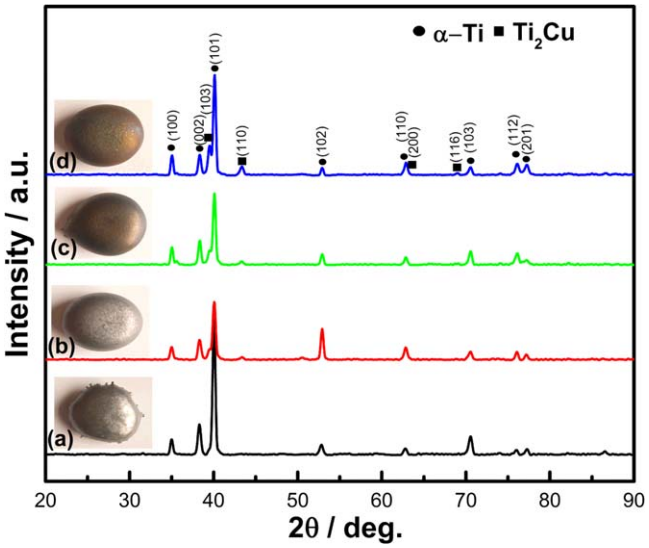

Figure 1. XRD patterns of the Ti-Cu alloy: (a) Ti-2Cu, (b) Ti-5Cu, (c) Ti-7Cu, (d) Ti-10Cu.

standard. The antibacterial rate R was calculated by the following equation(1):

$$R = (N_{control} - N_{sample})/N_{control} \times 100\% \quad (1)$$

Where, $N_{control}$ and N_{sample} were the average numbers of the bacterial colony on the control sample (CP-Ti) and the Ti-Cu samples, respectively.

3. Results and discussion

3.1. Phase identification

Figure 1 shows the XRD patterns of Ti-Cu alloys with different Cu content. Only the obvious diffraction peak of Ti was observed in the diffraction patterns of 2 wt.% Cu, as shown in figure 1(a). With the increase of Cu content, as shown in figures 1(b) to 1(d), the diffraction peak intensity of Ti_2Cu phase increased. This indicated that the precipitation of Ti_2Cu phase increased with the increase of Cu content. Interestingly, the diffraction peak intensity of α-Ti also increased with increasing Cu content from 5 to 10 wt.%.

Cu was a typical eutectoid-forming element in Ti binary alloy systems where $\beta \rightarrow \alpha + Ti_2Cu$ at 790 °C. According to the Ti-Cu binary phase diagram, only Ti_2Cu phase was synthesized as a secondary phase in Ti-Cu alloy with less than 40 wt.% Cu under an equilibrium solidification condition [20]. However, only α-Ti diffraction peak was detected in 2 wt.% Cu because the x-ray diffraction analysis did not succeed in detecting small volume fractions of Ti_2Cu phase. Otherwise, it was generally believed that the difference of atomic diameter between alloying element and matrix element was less than 16%, easily inducing diffusion between them [21]. Thus, the diffusion phenomenon between Ti and Cu would occur because the atomic diameter of Ti was about 13% larger than that of Cu. During the heat treatment, slow cooling resulted in the diffusion between Ti and Cu atoms and the formation of microstructure composed of α-Ti phase and precipitated Ti_2Cu phase in the Ti-Cu alloy. However, partial Cu atoms could diffuse into Ti matrix to form solid solution with α-Ti as the diffusion coefficient of Cu was larger than that of Ti under the action of thermal activation energy. Therefore, the excess Cu content, reaching at 10 wt.%, could promote the formation of α-Ti. In brief, the diffusion and reaction of Cu atoms would affect the morphology and distribution of microstructure.

3.2. Microstructure

The microstructure of Ti-Cu alloys with different Cu content is shown in figure 2. Although at low Cu concentrations of 2 wt.%, the white phases precipitated along the grain boundary of gray matrix (figure 2(a)). As the Cu content increased to 5 wt.%, the obvious changes that the white lamellar precipitates increased was observed, as shown in figure 2(b). These lamellar precipitates converged into many strip-like regions, which separated the matrix. Adding Cu content to 7 wt.% at eutectoid point, the eutectoid transformation occurred. Hereafter, the strip-like regions of the Ti-7Cu alloy increased, the lamellar distance between them decreased (figure 2(c)). Furthermore, the lamellar precipitates of the Ti-7Cu alloy (The inset of figure 2(c)) became longer than those of the Ti-5Cu alloy (The inset of figure 2(b)). As the concentration of Cu increased to 10 wt.% Cu, the

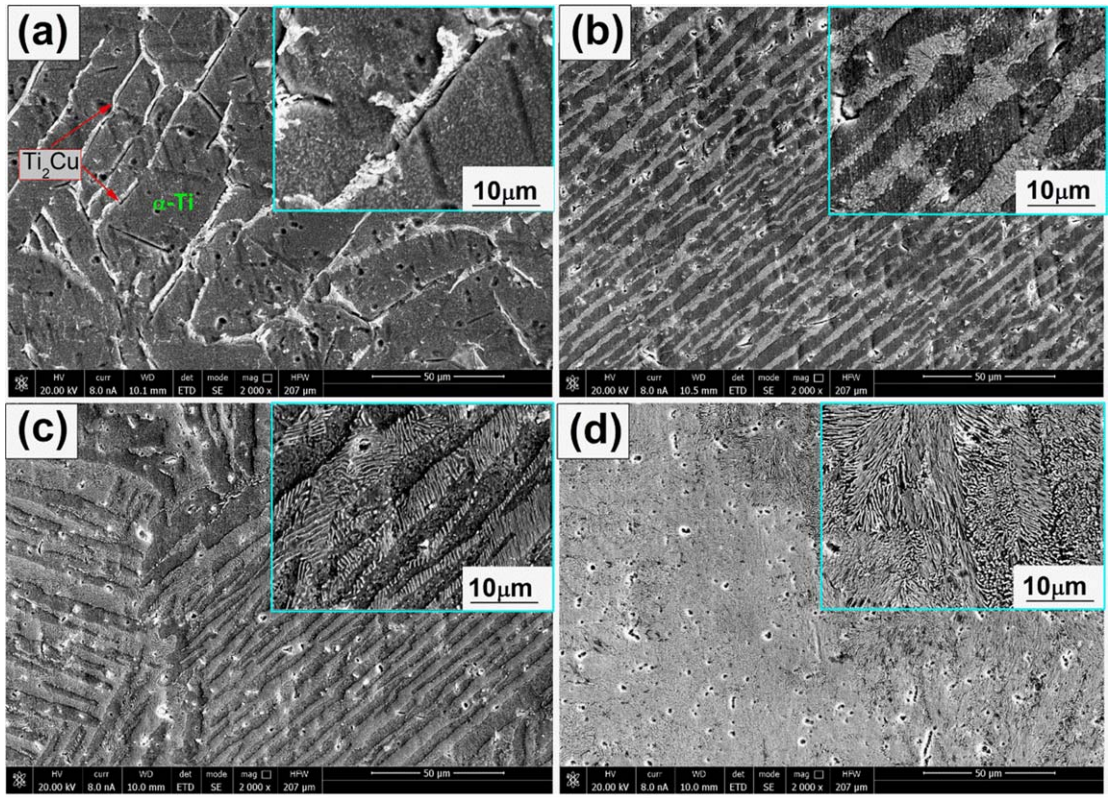

Figure 2. Microstructure characterization of the Ti-Cu alloy: SEM images of Ti-Cu alloys. (a) Ti-2Cu, (b) Ti-5Cu, (c) Ti-7Cu, and (d) Ti-10Cu.

hypereutectoid reaction occurred, which induced the finer eutectoid lamellae dispersed on the whole matrix of Ti-10Cu alloy. Thus, the Ti-10Cu alloy was covered by numerous lamellar precipitates, exhibited in figure 2(d).

During the heating process, the Ti-Cu alloy was mainly composed of a relevant amount of β phase and a certain amount of Ti_2Cu after the heat treatment temperature decreased to about 900 °C [16]. Upon slow cooling in the furnace, the decomposition of β phase induced the formation of α phase or eutectoid structure. The slower cooling rate was, the more eutectoid reaction occurred. Besides, the eutectoid reaction of the Ti-Cu alloy would be so active that the β-Ti phase was not retained due to the rapid diffusion of Cu into Ti [22]. Thus, the eutectoid reaction resulted in the precipitation of Ti_2Cu along the crystal boundary of α-Ti during the cooling process.

To further identify the composition of strip-like region, a map scanning was carried out on the element distribution of Ti-7Cu alloy by EPMA in figure 3. It was clearly seen that the distribution of Ti and Cu elements was exhibited in the mapping. The strip-like region was the enrichment area of Cu. Combining with the phase analysis of XRD, it can be deduced that the gray area was composed of α-Ti phases, while the strip-like region as eutectoid structure was composed of α-Ti and Ti_2Cu phases. The white lamellar structure could be identified as Ti_2Cu phases. The α-Ti phase as gray lamellar phase mainly distributed between the white lamellar structures. In any case, the microstructure of Ti-Cu alloy was affected by the Cu content and the heat treatment, which could cause differences in terms of mechanical properties.

3.3. Mechanical properties

As is well-known, the mechanical properties of Ti-Cu alloy can be improved by controlling Ti_2Cu precipitation [23]. Such precipitation could be achieved in response to Cu addition and heat treatment at 950 °C under vacuum condition. Table 1 shows summary of the mechanical properties of the Ti-Cu alloys. According to the data given in the table, the hardness of Ti-Cu alloy increased as the increase of Cu content. It was worth noting that the hardness of the Ti-Cu alloy, except for the Ti-2Cu alloy, was higher than that of Ti-20Ag alloy (230 HV) and Ti-5Cu alloy (270 HV) [16]. Due to the difference of diameters between Ti and Cu atom, the solid solution crystal lattice suffered serious distortion, which resulted in the slip surface becoming 'rough' and increased the resistance of dislocation motion, thus improving the hardness of the alloy. It was deduced that the increase of hardness was caused by solid-solution hardening of α-Ti and the precipitation of Ti_2Cu phase [24].

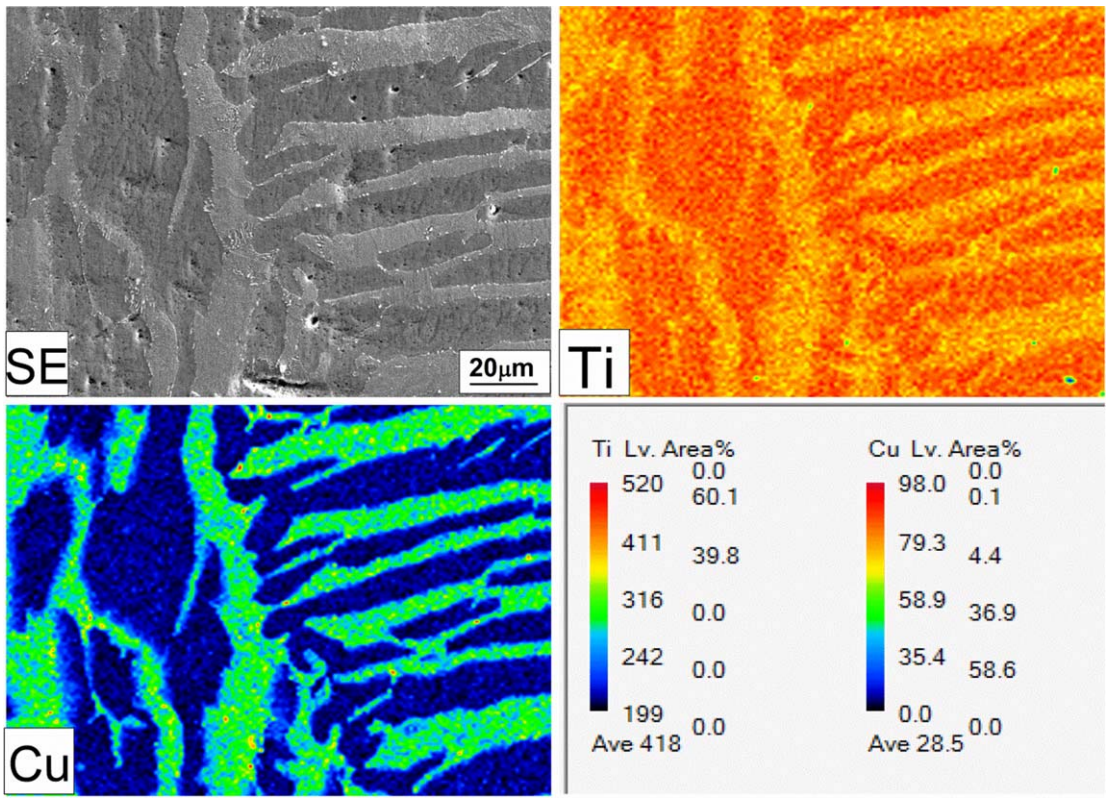

Figure 3. EPMA mapping scanning results of the Ti-7Cu alloy.

Table 1. Summary of mechanical properties of the Ti-Cu alloys: compressive strength σ_{max}, δ_e elastic energy δ_e, elastic modulus E, fracture strain εf, and Vickers hardness Hv.

Alloys	σ_{max} (MPa)	δ_e (MJ m^{-3})	ε_f(%)	B/GPa	G/GPa	E/GPa	B/G	Hv
Ti-2Cu	2034	8.17	68.6	114.3	47.3	124.6	2.42	217.3
Ti-5Cu	2045	6.45	68.7	106.1	47.1	123.1	2.25	255.3
Ti-7Cu	2169	12.76	60.6	104.0	40.9	108.4	2.54	292.6
Ti-10Cu	1828	12.87	55.9	135.1	45.9	123.8	2.94	343.5

Figure 4 shows the mechanical behavior and fracture morphology of the Ti-Cu alloy. In figure 4(a), the compressive strength of the alloy increased firstly and then decreased with the increase of Cu content. As seen from table 1, the Ti-7Cu alloy exhibited the highest compressive strength (2169 MPa), which was significantly higher than that of sintered Ti-10Cu alloy [13]. It indicated that the strength of the Ti-Cu alloy would be improved through the precipitated Ti_2Cu precipitated phase. However, the compressive strength of Ti-10Cu alloy decreased due to the increase of α-Ti phases, depicted in figure 1. That, the CP-Ti with single α-Ti phase displayed lower strength compared with conventional Ti alloy. In addition, it was worth noting that the fracture strain (ε_f) decreased with the increase of Cu content, indicating that the existence of precipitated Ti_2Cu phase led to the decrease of the ductility of Ti-Cu alloy. Obviously, the compressive strength of Ti-Cu alloy could be improved appreciably at the cost of a decrease in their ability to undergo plastic deformation. Even so, all of Ti-Cu alloys via heat treatment revealed high fracture strain ($\varepsilon_f > 55\%$) in the table 1, which were much higher than those of Ti-Cu alloys prepared by sintering ($\varepsilon_f < 30\%$) [13, 25] and casting ($\varepsilon_f < 25\%$) [26]. Briefly, the results revealed that the fracture strain of the Ti-Cu alloys could be substantially improved via heat treatment.

The biomedical materials implanted into human body was usually used under the condition of elastic deformation, which would bear heavy load [27]. Therefore, the elastic energy was worth to explore. As seen from the inset of figure 4(a), the elastic energy (δ_e) was expressed by the elastic deformation region of the stress-strain curve. The elastic energy could be calculated by the following formula [28]:

$$\delta_e = \frac{\varepsilon_e \sigma_y}{2} = \frac{\sigma_y^2}{2E} \tag{2}$$

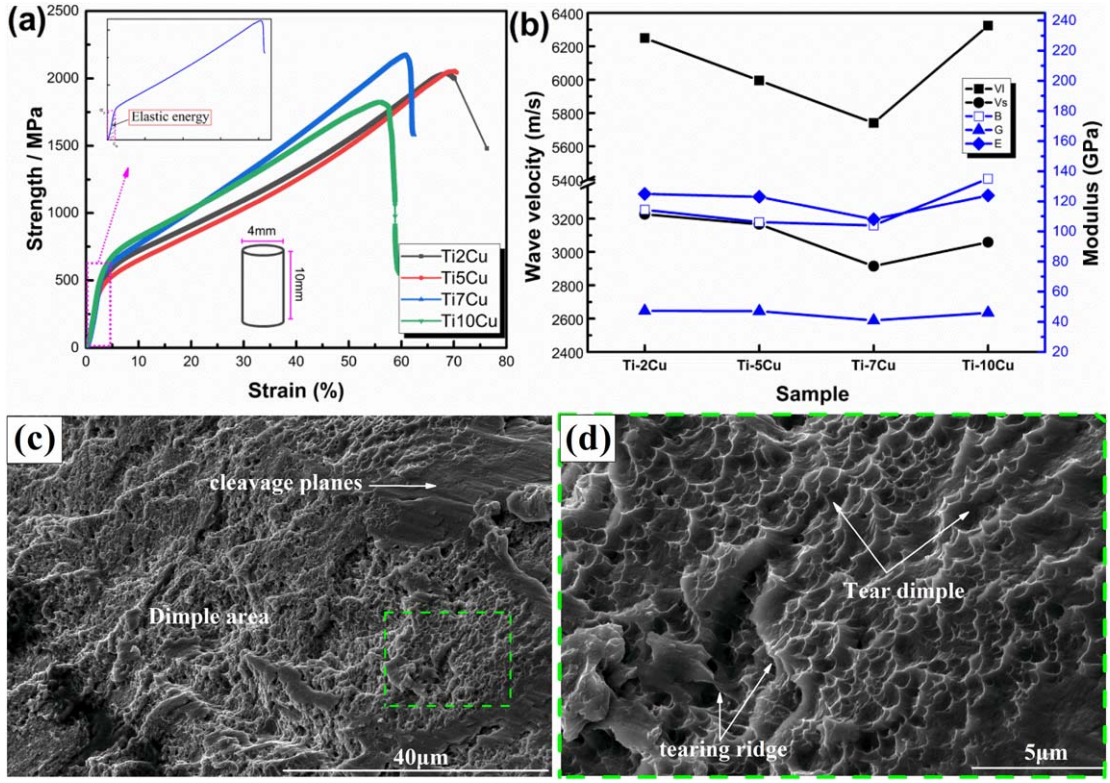

Figure 4. The mechanical behavior and fracture morphology of the Ti-Cu alloy. (a) typical stress-strain curve, (b) elastic modulus E, shear modulus G, bulk elastic modulus B, S-wave sound velocity versus and P-wave sound velocity curves V_b, (C) and (d) fracture SEM images with surface details of the sample with 7% Cu.

Where ε_e was the elastic strain, σ_y was the yield strength, and E was the elastic modulus of alloys in the stress-strain curve. According to the equation (2), the elastic energy of the prepared Ti-Cu alloys were ranged from 6.45 to 12.87 MJ m^{-3}, which was much higher than that of CP-Ti (about 2 MJ m^{-3}) and TC4 (about 3 MJ m^{-3}) [27]. It was deduced that the elastic energy of the Ti-Cu alloy would meet higher biosecurity when used as implants.

The modulus is an indispensable design value when used to compute deflections of prostheses by structural mechanics [29]. Thus, the moduli of Ti-Cu alloy were detected by Ultrasonic method, considered as a nondestructive and accurate technique, in determining a material's elastic constant. Firstly, the shear wave velocity (V_s) and the longitudinal wave velocity (V_l) were measured as the two basic physical quantities in the inset table of figure 4(b), and then the elastic moduli were calculated by the following formula [30]:

$$B = \rho \cdot (V_l^2 - 4Vs^2/3), \tag{3}$$

$$G = Vs^2 \cdot \rho, \tag{4}$$

$$E = 9B \cdot G/(3B + G) \tag{5}$$

Where, B and G were the bulk modulus and shear modulus (GPa), ρ was the density of Ti-Cu alloy (kg m^{-3}), respectively. According to the equations (3)–(5), the values of G, B and E of the alloy were calculated, depicted in table 1 and figure 4(b). It was seen from figure 4(b) that the change trends of B and G were similar with that of E. The Ti-7Cu alloy composed of Ti_2Cu and α-Ti phases, depicted a decrease in Young's modulus, possibly due to lower Young's modulus in the Ti_2Cu precipitated phase. It was considerable that the elastic modulus of Ti-7Cu alloy (108GPa) was lower than that of Ti-7.1Cu alloy (120GPa), which would be beneficial to reduce stress shielding effect. However, the elastic modulus of Ti-10Cu alloy increased because of the increase of α-Ti phases. Besides, the ratio B/G was used as an indicator of ductility or brittleness of compound. As seen from table 1, the ratios B/G were 2.42, 2.25, 2.54 and 2.94 for Ti-2Cu, Ti-5Cu, Ti-7Cu and Ti-10Cu alloy, respectively. It was obviously that the ratios of all of Ti-Cu alloy were over 1.75, indicating good toughness. This result was also consistent with high fracture strain measured by the compressive test.

The fracture morphology of the Ti-7Cu alloy was displayed in figures 4(c) and 4(d). The fracture morphology was mainly composed of dimples, cleavage plane and tearing ridge, displaying that the alloy possessed good plastic strain. The fracture with partially enlarged dimple characteristics was shown in figure 4(d). The tearing dimple could be observed clearly generated under the combination of shear stress and

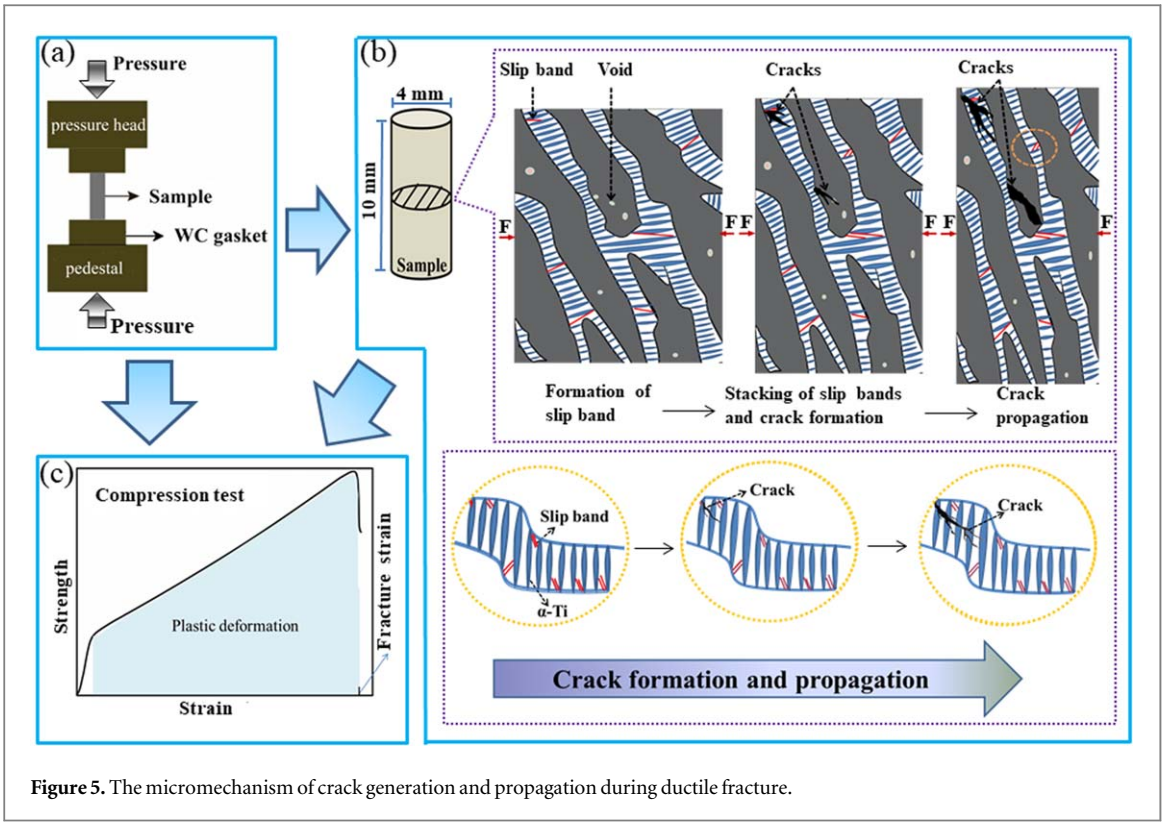

Figure 5. The micromechanism of crack generation and propagation during ductile fracture.

bending stress, but no grain boundaries were found in the fracture morphology. Therefore, it could be inferred that the fracture mechanism mainly belonged to ductile fracture.

The micromechanism of crack formation and propagation during ductile fracture is conceptualized schematically in figure 5. During the compression (figure 5(a)), lots of dislocations appeared and gathered to form the slip band (figure 5(b)). As the elastic deformation evolved, the stacking of slip band would be further intensified, and the origin of crack happened along the hard phases (Ti_2Cu phase) [31] and some voids. Those voids could be engendered by some pores and precipitated inclusions in the alloy. When the plastic deformation stage occurred, the stress and strain concentration along a certain slip band induced the crack propagation of the Ti-Cu alloy. The white lamellar Ti_2Cu phases uniformly distributed on the eutectoid structure, would accelerate crack propagation, but α-Ti as a plastic phase [32] delay the crack propagation to improve the plastic strain of Ti-Cu alloy. Therefore, the lamellar structure with the alternate plastic phases and brittle phases would prevent crack propagation.

Therefore, the proper lamellar structure would increase the deformation resistance and exhibit excellent fracture strain of the Ti-Cu alloy (figure (5c)).

3.4. Corrosion properties

The addition of Cu into pure Ti induced excellent improvements in mechanical properties. However, it is well known that the corrosion resistance and biocompatibility was hindered by alloying, depending on the used element [33]. In order to estimate the corrosion resistance of Ti-Cu alloy, the electrochemical measurement was executed, the typical open-circuit potential curves and Tafel curves of Ti-Cu alloys in Hank's solution are represented in figure 6. The electrochemical data obtained from the open-circuit potential and Tafel curves are summarized in table 2.

Compared with Ti-2Cu and Ti-5Cu alloy, open-circuit potential in the initial stage of open-circuit potential curves for the Ti-7Cu and Ti-10Cu alloys increased and reached a stable level as the immersion time increasing, indicating that a passive film was formed on the surface of the Ti-Cu alloys (figure 6(a)). In the anodic active region of Tafel curves, all of Ti-Cu alloys displayed a stable passivation region and unique passive-active behavior, and showed obvious passivation characteristics, indicating that passivation film was formed on the surface of these samples. However, the Ti-7Cu and Ti-10Cu alloys exhibited more positive corrosion potential (E_{corr}) than those of Ti-2Cu and Ti-5Cu alloy (figure 6(b)). Certainly, the corrosion rate (V) would determine corrosion resistance. According to Faraday's law:

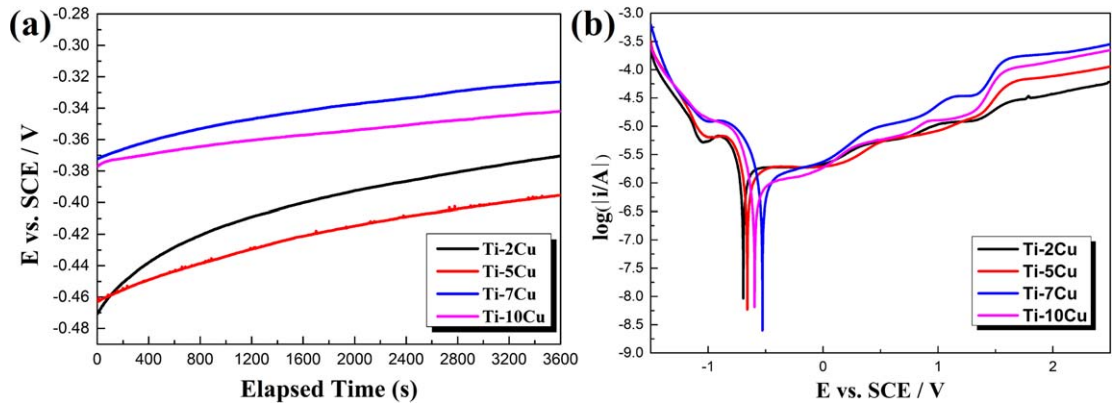

Figure 6. Typical OCP (a) and Tafel curves (b) of the Ti-Cu alloys.

Table 2. Electrochemical data of the Ti-Cu alloys.

Alloys	E_{corr}(V)	i_{corr} (μA·cm^{-2})	R_p (kΩ·cm^{-2})	β_a (mV)	β_c (mV)
Ti-2Cu	−0.694	2.061	30.954	1.964	4.850
Ti-5Cu	−0.662	1.496	36.755	2.536	5.373
Ti-7Cu	−0.525	0.749	57.524	2.603	7.491
Ti-10Cu	−0.598	0.969	48.894	2.826	6.344

$$V = i_{\text{corr}} \cdot \frac{A}{nF} \tag{6}$$

Where, i_{corr} was the corrosion current density; A was the relative atomic mass of metal; n was the valence number of metal ions; F was the Faraday constant, respectively. As seen from equation (6), the corrosion rate was proportional to the corrosion current density during the corrosion process. The lower the corrosion current density was, the lower the corrosion rate was, demonstrating that the passivation film on the surface was better able to protect the material.

Therefore, the value of corrosion current density (i_{corr}) would be a more important indicator of corrosion resistance for metal material. The i_{corr} was obtained using Stern-Geary equation [34]:

$$i_{corr} = \frac{\beta_a \cdot \beta_c}{2.3R_p(\beta_a + \beta_c)} \tag{7}$$

Where, β_a and β_c were the Tafel slopes of the anodic and cathodic part of Tafel plot and R_p was linear polarization resistance. The values of E_{corr}, i_{corr}, β_a, β_c and R_p were shown in table 2. The values of i_{corr} decreased with the increase of Cu content. The i_{corr} values of the Ti-7Cu and Ti-10Cu alloys were 0.749 and 0.969 μA·cm^{-2}, respectively. Compared with TC4 (5.86 $\pm$ 0.98 μA·cm^{-2}) [35], the Ti-7Cu and Ti-10Cu alloys exhibited higher corrosion resistance due to the precipitated Ti_2Cu phases increasing [13], which could promote the formation of passive film on the surface of the Ti-Cu alloy.

3.5. Antibacterial activity

Figure 7 shows the typical colonies of *S. aureus* and *E. coli* cultured on the sample surface for 24 h. A large number of bacteria were observed on CP-Ti and Ti-2Cu samples, indicating the fact that neither sample had antibacterial property. On the contrary, little bacterial colony including *E. coli* and *S. aureus* bacteria could be found on the Ti-7Cu and Ti-10Cu samples, demonstrating that these Ti-Cu alloys had good antibacterial property (figure 7(a)).

The antibacterial rate of the Ti-Cu alloy was calculated and depicted in figure 7(b). According to figure 5(b), the Ti-7Cu and Ti-10Cu alloy with the antibacterial rate of over 99% exhibited strong antibacterial properties according to *GB/T 4789.2–2016* Standard. Based on these results, it could be seen that the Cu content had a great influence on the antibacterial property.

Although the bacteria required low concentrations of Cu ions as essential micronutrients, even so, high concentrations of Cu ions could inhibit cell growth or even lead to cell death [36]. When the bacteria colony of *E. coli* and *S. aureus* was cultured in the Ti-Cu alloy for 24 h, Cu ions could be released from the precipitated Ti_2Cu phases [37]. With the increase of Cu content, the release of Cu ions increased. The released Cu ions firstly contacted with the bacterial cell membrane, resulting in local oxidation or short circuit on the surface [38].

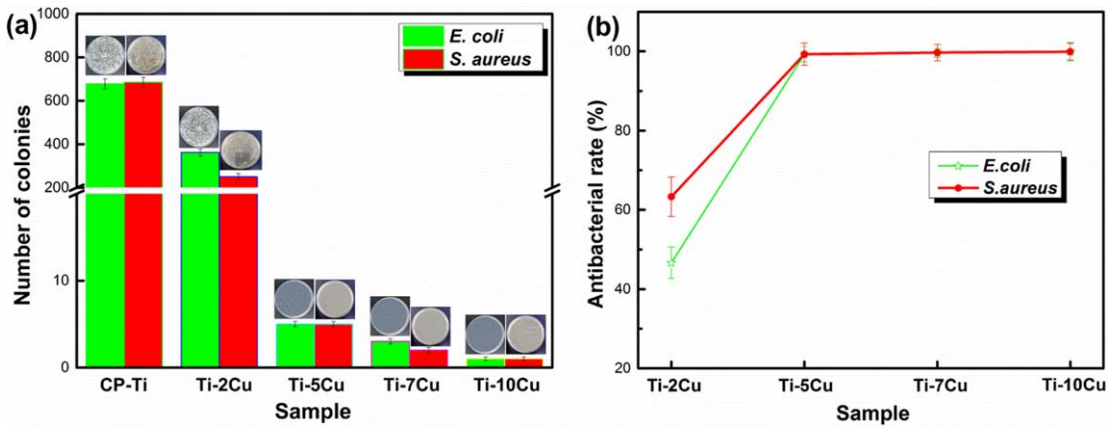

Figure 7. Antibacterial properties of the Ti-Cu alloys against *E. coli* and *S. aureus*. (a) Numbers of bacteria colonies co-cultured with the samples; (b) Antibacterial rate co-cultured with the samples.

When the cell membrane of bacteria was destroyed, the Cu ions would react with bacterial proteins so as to kill the bacteria. Therefore, the Cu content of Ti-Cu alloy could be a direct impact on antibacterial activity.

4. Conclusions

The Ti-*x*Cu ($x = 2, 5, 7, 10$ wt.%) alloy was successfully prepared by combing Ar-arc melting technology with heat treatment method. The Ti-Cu alloy was mainly composed of α-Ti and Ti_2Cu. With the increase of Cu content, the Ti_2Cu precipitation phase increased, which induced high strength and low elastic modulus for Ti-7Cu alloy, and improved the corrosion resistance for Ti-7Cu alloy and Ti-10Cu alloy. The antibacterial test illuminated that the Ti-Cu alloy with more than 5 wt.% Cu, possessed strong antibacterial property against *E. coli* and *S. aureus*. Therefore, it could be concluded that the Ti-Cu alloys, especially for Ti-7Cu alloy, would be a very proper substitute for biomedical implant materials due to its very high strength, low modulus, high fracture strain, excellent corrosion resistance and antibacterial property.

Acknowledgments

This study was funded by the National Natural Science Foundation of China (31660262), and the Key Research and Development Project of Yunnan (2018BA064).

ORCID iDs

ZhengYuan He https://orcid.org/0000-0001-7113-2930

References

[1] Chen Q Z and Thouas G A 2015 Metallic implant biomaterials *Mat. Sci. Eng. R* **87** 1–57
[2] Vilarrasa J, Delgado L M, Galofre M, Alvarez G, Violant D, Manero J M, Blanc V, Gil F J and Nart J 2018 *In vitro* evaluation of a multispecies oral biofilm over antibacterial coated titanium surfaces *J. Mater. Sci., Mater. Med.* **29** 164
[3] Mombelli A, Schmid B, Rutar A and Lang N P 2002 Local antibiotic therapy guided by microbiological diagnosis - treatment of porphyromonas gingivalis and actinobacillus actinomycetemcomitans persisting after mechanical therapy *J. Clin. Periodontol.* **29** 743–9
[4] Hou L, Li L and Zheng Y 2013 Fabrication and characterization of porous sintered Ti–Ag compacts for biomedical application purpose *J. Mater. Sci. Technol.* **29** 330–8
[5] Huang T C, Chen C J, Ding S J and Chen c.c. 2019 Antimicrobial efficacy of methylene blue-mediated photodynamic therapy on titanium alloy surfaces *in vitro Photodiagn Photodyn.* **25** 7–16
[6] Secinti K D, Ayten M, Kahilogullari G, Kaygusuz G, Ugur H C and Attar A 2008 Antibacterial effects of electrically activated vertebral implants *J. Clin. Neurosci.* **15** 434–9
[7] Grass G, Rensing C and Solioz M 2011 Metallic copper as an antimicrobial surface *Appl. Environ. Microb.* **77** 1541–7
[8] Nowak A, Szade J, Talik E, Zubko M, Wasilkowski D, Dulski M, Balin K, Mrozik A and Peszke J 2016 Physicochemical and antibacterial characterization of ionocity Ag/Cu powder nanoparticles *Mater. Charact.* **117** 9–16
[9] Wan Y Z, Xiong G Y, Liang H, Raman S, He F and Huang Y 2007 Modification of medical metals by ion implantation of copper *Appl. Surf.* **253** 9426–9

[10] Azeena S, Subhapradha N, Selvamurugan N, Narayan S, Srinivasan N, Murugesan R, Chung T W and Moorthi A 2017 Antibacterial activity of agricultural waste derived wollastonite doped with copper for bone tissue engineering *Mat. Sci. Eng. C-Mater.* **71** 1156–65
[11] Kang B M, Jeong W-J, Park G-C, Yoon D-J, Ahn H-G and Lim Y-S 2015 The characteristics of an antibacterial TiAgN thin film coated by physical vapor deposition technique *J. Nanosci. Nanotechno.* **15** 6020–3
[12] Norambuena G *et al* 2017 Antibacterial and biocompatible titanium-copper oxide coating may be a potential strategy to reduce periprosthetic infection: an *in vitro* study *Clin. Orthop. Relat. R.* **475** 722–32
[13] Zhang E, Li F, Wang H, Liu J, Wang C, Li M and Yang K 2013 A new antibacterial titanium–copper sintered alloy: preparation and antibacterial property *Sci. Eng. C-Mater.* **33** 4280–7
[14] Wang X, Dong H, Liu J, Qin G, Chen D and Zhang E 2019 *In vivo* antibacterial property of Ti-Cu sintered alloy implant *Mat. Sci. Eng. C-Mater.* **100** 38–47
[15] Shi H, Ye X, He F and Ye J 2019 Improving osteogenesis of calcium phosphate bone cement by incorporating with lysine: an *in vitro* study *Colloid. Surface. B.* **177** 462–9
[16] Takahashi M, Kikuchi M, Takada Y and Okuno O 2002 Mechanical properties and microstructures of dental cast Ti-Ag and Ti-Cu alloys *Dent. Mater. J.* **21** 270–80
[17] Guo S *et al* 2017 Preliminary study on the corrosion resistance, antibacterial activity and cytotoxicity of selective-laser-melted Ti6Al4V-xCu alloys *Mat. Sci. Eng. C-Mater.* **72** 631–40
[18] Li Y-H, Chen N, Cui H-T and Wang F 2017 Fabrication and characterization of porous Ti–10Cu alloy for biomedical application *J. Alloy. Compd.* **723** 967–73
[19] Zhang L, Zhao G, Tan J, He Z Y and Jiang Y H 2018 Electrochemical behavior in simulated physiological solution of Ti-Nb-Zr-calcium pyrophosphate composite with enhanced bioactivity by spark plasma sintering *J. Electrochem. Soc.* **165** E221–30
[20] Okamoto H 1994 Comment on Cu-Ti (copper-titanium) *J. Phase Equilib.* **15** 566–7
[21] Chen Z Q, Li Y, Hu D, Loretto M and Wu X 2003 Role of alloying elements in microstructures of beta titanium alloys with carbon additions *J. Mater. Sci. Technol.* **19** 1391–8
[22] Taguchi O and Iijima Y 1995 Diffusion of copper, silver and gold in α-titanium *Philos. Mag. A* **72** 1649–55
[23] Cardoso F F, Cremasco A, Contieri R J, Lopes E S N, Afonso C R M and Caram R 2011 Hexagonal martensite decomposition and phase precipitation in Ti–Cu alloys *Mater. Des.* **32** 4608–13
[24] Kikuchi M, Takada Y, Kiyosue S, Yoda M, Woldu M, Cai Z, Okuno O and Okabe T 2003 Mechanical properties and microstructures of cast Ti-Cu alloys *Dent. Mater.* **19** 174–81
[25] Dong R, Zhu W, Zhao C, Zhang Y and Ren F 2018 Microstructure, mechanical properties, and sliding wear behavior of spark plasma sintered Ti-Cu alloys *Metall. Mater. Trans. A* **49** 6147–60
[26] Zhang E, Wang X, Chen M and Hou B 2016 Effect of the existing form of Cu element on the mechanical properties, bio-corrosion and antibacterial properties of Ti-Cu alloys for biomedical application *Mat. Sci. Eng. C-Mater.* **69** 1210–21
[27] Zhan Y, Li C and Jiang W 2012 β-type Ti-10Mo-1.25Si-xZr biomaterials for applications in hard tissue replacements *Mat. Sci. Eng. C-Mater.* **32** 1664–8
[28] Niinomi M 1998 Mechanical properties of biomedical titanium alloys *Mater. Sci. Eng. A-Struct* **243** 231–6
[29] Kikuchi M, Takahashi M and Okuno O 2006 Elastic moduli of cast Ti–Au, Ti–Ag, and Ti–Cu alloys *Dent. Mater.* **22** 641–6
[30] Fleischer R, Gilmore R and Zabala R 1988 Elastic moduli of polycrystalline, intermetallic compounds of titanium *J. Appl. Phys.* **64** 2964–7
[31] Wang J, Zhang S, Sun Z, Wang H, Ren L and Yang K 2019 Optimization of mechanical property, antibacterial property and corrosion resistance of Ti-Cu alloy for dental implant *J. Mater. Sci. Technol.* **35** 2336–44
[32] Zhang E, Li S, Ren J, Zhang L and Han Y 2016 Effect of extrusion processing on the microstructure, mechanical properties, biocorrosion properties and antibacterial properties of Ti-Cu sintered alloys *Mater. Sci. Eng. C-Mater.* **69** 760–8
[33] Okabe T, Kikuchi M, Ohkubo C, Koike M, Okuno O and Oda Y 2004 The grindability and wear of Ti-Cu alloys for dental applications *JOM* **56** 46–8
[34] Stern M and Geaby A L 1957 Electrochemical polarization *J. Electrochem. Soc.* **104** 56
[35] Bao M, Wang X, Yang L, Qin G and Zhang E 2018 Tribocorrosion Behavior of Ti–Cu Alloy in Hank's Solution for Biomedical Application *Journal of Bio-and Tribo-Corrosion* **4** 29
[36] Zhu L, Elguindi J, Rensing C and Ravishankar S 2012 Antimicrobial activity of different copper alloy surfaces against copper resistant and sensitive Salmonella enterica *Food Microbiol.* **30** 303–10
[37] Zhang E L, Ren J, Li S Y, Yang L and Qin G W 2016 Optimization of mechanical properties, biocorrosion properties and antibacterial properties of as-cast Ti-Cu alloys *Biomed. Mater.* **11** 13
[38] Ke Z, Yi C, Zhang L, He Z, Tan J and Jiang Y 2019 Characterization of a new Ti-13Nb-13Zr-10Cu alloy with enhanced antibacterial activity for biomedical applications *Mater. Lett.* **253** 335–8